applied sciences

MDPI

Article

Nickel (Ni^{2+}) Removal from Water Using Gellan Gum–Sand Mixture as a Filter Material

Thi Phuong An Tran [1,†], Hoon Cho [2,†], Gye-Chun Cho [3,*], Jong-In Han [3] and Ilhan Chang [4,*]

1 Department of Hydrological and Geotechnical Engineering, University of Sciences, Hue University, Hue 49000, Vietnam; ttphuongan@hueuni.edu.vn
2 Samsung Electronics Semiconductor R&D Center, 1-1 Samsungjeonja-ro, Hwaseong-si 18448, Korea; hoonchamp@gmail.com
3 Department of Civil and Environmental Engineering, Korea Advanced Institute of Science and Technology (KAIST), Daejeon 34141, Korea; jihan@kaist.ac.kr
4 Department of Civil Systems Engineering, Ajou University, Suwon 16499, Korea
* Correspondence: gyechun@kaist.edu (G.-C.C.); ilhanchang@ajou.ac.kr (I.C.); Tel.: +82-42-350-3622 (G.-C.C.); +82-31-219-2503 (I.C.)
† Equal contribution: T.P.A.T. and H.C.

Abstract: Microbial biopolymers have been introduced as materials for soil treatment and ground improvement purposes because of their ability to enhance soil strength enhancement and to reduce hydraulic conductivity. Several studies in the field of environmental engineering have reported heavy metal adsorption and removal from contaminated water using common biopolymers. In particular, gellan gum biopolymers have drawn significant attention for use in metal ion adsorption. This study aims to investigate the heavy metal adsorption capacity of a gellan gum biopolymer–sand mixture when nickel-contaminated water is pumped upward through a uniform gellan gum–sand mixture column. The main aims of this study are (1) to clarify the Ni^{2+} adsorption phenomenon of gellan gum-treated sand, (2) to assess the Ni^{2+} adsorbability of gellan gum–sand mixtures with different gellan gum content, and (3) to examine the gellan gum–sand filter thickness and flow rate effects on Ni^{2+} adsorption. The results of this experiment demonstrate the effectiveness of gellan gum in terms of Ni^{2+} adsorption and water flow rate control, which are essential criteria of a filter material for contaminated water treatment.

Keywords: gellan gum; hydraulic conductivity; water absorption; metal ion adsorption; pore-clogging

Citation: Tran, T.P.A.; Cho, H.; Cho, G.-C.; Han, J.-I.; Chang, I. Nickel (Ni^{2+}) Removal from Water Using Gellan Gum–Sand Mixture as a Filter Material. *Appl. Sci.* **2021**, *11*, 7884. https://doi.org/10.3390/app11177884

Academic Editor: Bart Van der Bruggen

Received: 2 August 2021
Accepted: 24 August 2021
Published: 26 August 2021

1. Introduction

Heavy metals dissolved in water can lead to bioaccumulation and might pose a risk to human health when consumed through the food chain [1,2]. To protect soil and groundwater from adjacent contamination sources (e.g., municipal waste landfills, and agricultural and industrial wastewater), hydraulic barriers have been actively applied in practice. In general, hydraulic barriers use inorganic adsorbents, organic adsorbents, and biosorbents owing to their properties of hydraulic conductivity reduction, high shear strength, and high contaminant removal capacities [3,4].

Recently, multiple studies have suggested biosorption as an eco-friendly approach for aqueous contaminant removal [5–8] and ground hydraulic conductivity control [9,10]. The principal mechanism of ion adsorption involves the formation of complexes between a metal ion and functional groups (carboxyl, carbonyl, amino, sulfonate, and phosphate), which are present on the surface or inside the porous structure of biological materials [11]. Furthermore, the hydrophilicity of biopolymers that form hydrogen bonds with water molecules [12] results in pore-clogging, mitigating fluid flow, and transport through porous media [13].

In this study, nickel (Ni^{2+}) and gellan gum (GG) were used to investigate the Ni^{2+} adsorption and removal capability of GG biopolymer–sand mixtures. GG is known as an

effective material for soil strength enhancement and hydraulic conductivity reduction [9,14]. Nickel metal is an allergen [15] and a potential immunomodulatory and immunotoxic agent for humans [16]. Furthermore, clinical studies on humans and animals exposed to Ni^{2+} concluded that Ni^{2+} is carcinogenic to humans [17]. A previous study demonstrated the effectiveness of GG for Ni^{2+} removal compared with that of other polymeric materials (Figure 1) [6]. However, Ni^{2+} adsorption and removal from an aqueous Ni^{2+} solution has not been clearly investigated. Therefore, it is crucial to study the adsorption of Ni^{2+} ion by GG biopolymer to assess the feasibility of using a GG–sand mixture as a filter or hydraulic barrier material to ensure sustainable development.

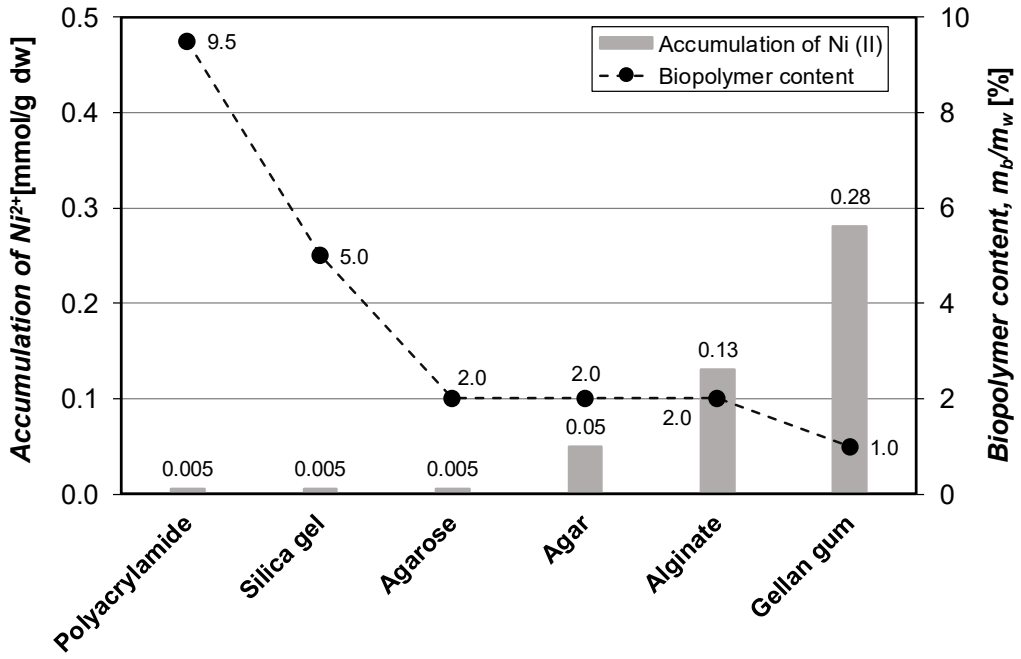

Figure 1. Nickel adsorption of different biopolymers [6].

2. Materials and Experimental Preparation

2.1. Materials

2.1.1. Sand (Jumunjin Sand)

Jumunjin sand, which is the standard sand in Korea, was used in this study. Jumunjin sand is classified as a poorly graded sand with a particle size distribution of D_{50} = 0.46 mm. It has a uniform coefficient (C_u) and a coefficient of gradation (C_c) of 1.39 and 0.76, respectively [14] (Figure 2).

2.1.2. GG Biopolymer

Thermo-gelated GG, which is a linear polysaccharide produced by the bacterium *Pseudomonas elodea*, has a repeating unit consisting of α-L-rhamnose, β-D-glucose, and β-D-glucuronate in the molar ratio 1:2:1 [18]. GG can be used for soil strengthening and hydraulic conductivity reduction [9,14]. A low acyl GG biopolymer supplied by Sigma Aldrich (CAS No.71010-52-1) was used in this study.

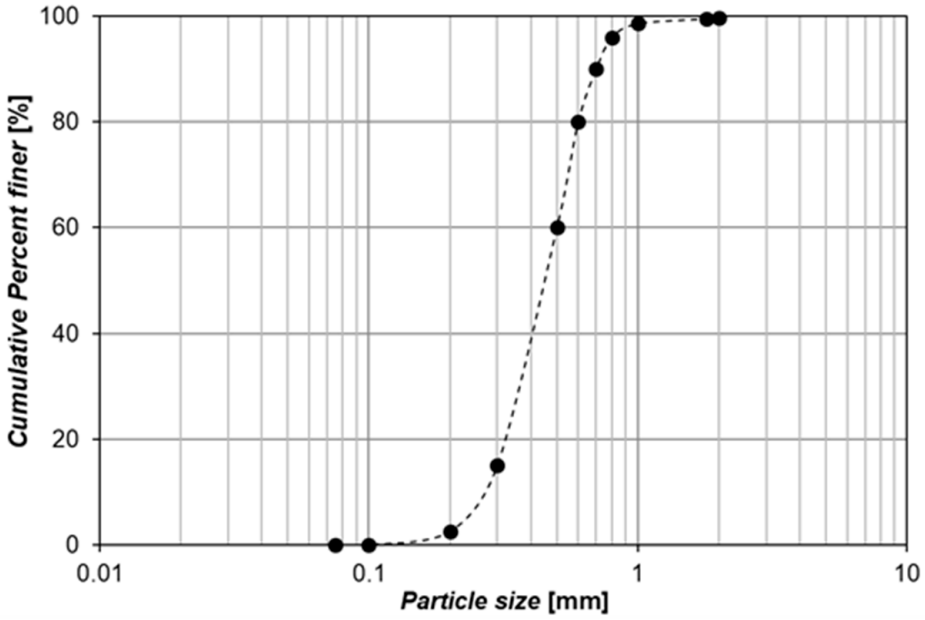

Figure 2. Particle size distribution of jumunjin sand.

2.1.3. GG-Treated Sand: Hydraulic Barrier Liner

The GG–soil mixtures were prepared with GG contents (to the mass of soil) of 0.5, 1.0, and 2.0%. To ensure thorough mixing, the initial water content was set at 35%. GG was dissolved and hydrated in deionized water heated at 100 °C to obtain a uniform GG solution. Jumunjin sand was washed, dried, and uniformly mixed with the heated GG solution. Subsequently, the GG–sand specimens were formed in a mold with a diameter of 3.5 cm and a height of 10 cm. The samples were allowed to cool down at room temperature (i.e., 20 °C). The GG-treated sand samples were trimmed to obtain a target height of 5 cm. The specimens were referred to as 0 HBL, 0.5 HBL, 1.0 HBL, and 2.0 HBL, corresponding to the GG content used to form the hydraulic barrier liner (HBL) of 0.0, 0.5, 1.0, and 2.0%, respectively. The dry densities of the specimens are mentioned in Table 1.

Table 1. Dry density of the specimens.

GG Content [%]	0.0	0.5	1.0	2.0
Symbol	0.0 HBL	0.5 HBL	1.0 HBL	2.0 HBL
Dry density [g/cm^3]	1.61	1.57	1.54	1.53

2.2. Experimental Process

2.2.1. Upward Flow System

The experimental flow system consisted of three main parts: a syringe pump, an acrylic cylinder (diameter of 3.5 cm; length of 12 cm), and a pressure data logger (Figure 3). Jumunjin sand was compacted in the acrylic column before setting the HBL on top of the specimen. The syringe pump pumped $NiCl_2.6H_2O$ solution from a 60 mL syringe to the soil column in the acrylic cylinder at a constant flow rate via the inlet system. The bottom and top caps include inlet and outlet systems. The solution from the outlet was collected to measure the change in hydraulic conductivity of the soil column and the Ni^{2+} removability of the soil column.

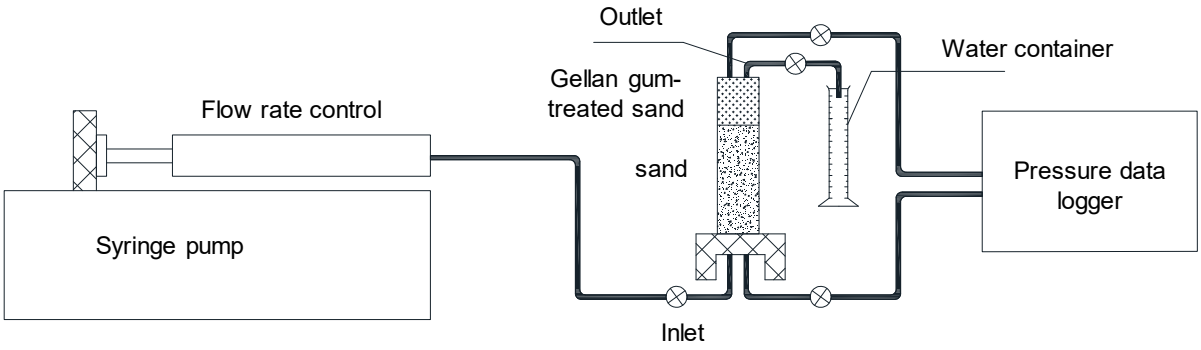

Figure 3. Schematic of the pressurized upward flow system.

The voltage values in mV, which were monitored at the top and bottom of the soil column by the pressure data logger, were converted to pressure (kPa), and then they were converted to head difference (m). The drained water was collected to measure its volume with testing time. The data of the head difference, the volume of water, and the time were collected and used to calculate the hydraulic conductivity of the soil column.

In this study, to demonstrate the action of HBL under adverse conditions, the HBL was fully saturated by an upward flow of $NiCl_2.6H_2O$ solution. The Ni^{2+} adsorption tests were conducted on saturated specimens. The experimental conditions are summarized in Table 2.

Table 2. Experimental test conditions.

Flow Rate [mL/min]	Thickness of HBL [cm]	GG Contents [%]			
0.04 0.20	5	0	0.5	1.0	2.0

2.2.2. Adsorbate Preparation

Nickel concentration in groundwater and municipal tap water in polluted areas was in the range of 100–2500 mg/L. Conversely, a nickel concentration greater than 1000 mg/L was found in the water boiled in electric kettles [19]. In this study, to mimic adverse conditions due to environmental pollution, an initial concentration of 1000 mg/L of $NiCl_2.6H_2O$ [20,21] was used.

2.2.3. Adsorption Isotherm and Kinetic Study

To study the nickel adsorption mechanism of the GG–sand mixture, an equilibrium isotherm study was conducted. Different concentrations of nickel (10–1000 mg/L) were used to determine the equilibrium isotherm. Samples (40 mL) with designated nickel concentrations were mixed with 5 g of GG-treated sand (0 HBL, 0.5 HBL, 1.0 HBL, and 2.0 HBL) in 50 mL Falcon tubes. The samples were mixed at 120 rpm at 25 °C for 24 h and filtered using a 0.45 µm nylon filter for further analysis.

The empirical equilibrium adsorption isotherm was modeled using the Langmuir and Freundlich isotherm equations. The adsorption isotherm provides insight about the interaction between the adsorbent and adsorbate. The Langmuir model is written as follows:

$$q_e = \frac{q_{\max} k_L C_e}{1 + k_L C_e}, \quad (1)$$

where q_e is the metal uptake per adsorbent (mg/g), q_{max} is the maximum adsorption, k_L is the Langmuir constant, and *Ce* is the equilibrium metal concentration (mg/L). Langmuir isotherm fitting indicates a monolayer process where the k_L can be a criterion of adsorbate affinity to the adsorbent. A high value of k_L indicates a strong interaction. Conversely, the Langmuir isotherm can be directly related to the homogenous surface with uniform adsorption energy.

The Freundlich equation is written as follows:

$$q_e = k_F C_e^{1/n}, \quad (2)$$

where k_F is the Freundlich constant and n is the empirical constant. Freundlich isotherm empirically considers a multi-layer coverage on rough surfaces. The model fitting of the experimental data was checked with the correlation coefficient R^2.

To understand the kinetic uptake of nickel adsorption with time, GG-treated sands with 25 mg/L, 50 mg/L, and 100 mg/L nickel solutions were tested and taken according to the desired time. The experimental conditions were the same as those mentioned above.

2.2.4. Adsorption Isotherm and Kinetic Study

Hydraulic Conductivity Analysis

The hydraulic conductivity is calculated using Darcy's law:

$$k = \frac{V \cdot L}{A \cdot h \cdot t}, \quad (3)$$

where V is the volume of water collected, L is the height of HBL, A is the area of the soil specimen, h is the head difference, and t is the time required to obtain V.

L is the height of HBL because the presence in HBL is the main factor governing the reduction in hydraulic conductivity.

Nickel Analysis

The concentration of nickel ions in the solution was measured using inductively coupled plasma-optical emission spectrometry (Agilent ICP-OES 5110, SCLA, USA), calibrated by the standard metal solution. The amount of nickel uptake (mg/g) was calculated using the following equation:

$$q_e = \frac{\left(C_i - C_f\right) \cdot V}{1000 \cdot W}, \quad (4)$$

where C_i and C_f are the nickel ion concentration at the initial and final stages, respectively (mg/L), W is the amount of adsorbent (g), and V is the volume of solution (mL). The removal efficiency (R, %) via nickel adsorption is calculated as follows:

$$R = \frac{C_i - C_f}{C_i} \cdot 100. \quad (5)$$

Surface Morphology

Scanning electron microscopy (SEM-SU5000, Hitachi, Japan) was performed on GG-treated sand samples after Ni^{2+} adsorption. The morphologies of the samples were observed using energy-dispersive X-ray spectroscopy (EDS) for element characterization. SEM-EDS was performed on ten points per sample to minimize deviations. In addition, the samples were coated with platinum before analysis to enhance the electrical conductivity of the surface.

3. Results and Analysis

3.1. Isotherm and Kinetics of Heavy Metal Adsorption Mechanism

Figure 4 shows the adsorption of nickel solution on each GG-treated sand specimen. The results show that GG and sand had the ability to adsorb nickel. All three conditions (sand, 0.5 HBL, and 1.0 HBL) show a logarithmic trend in the equilibrium state. The equilibrium uptake of nickel adsorbate increased with an increase in the GG content. Figure 4b,c show the Langmuir and Freundlich isotherm models, respectively. All three data were fitted better with the Langmuir isotherm model compared with that of the Freundlich isotherm model, with an R^2 value of 0.9881 to 0.9983 for the Langmuir model

(Figure 4b) and 0.782 to 0.9197 for the Freundlich model (Figure 4c). The parameters of the Langmuir model and the Freundlich model are summarized in Table 3.

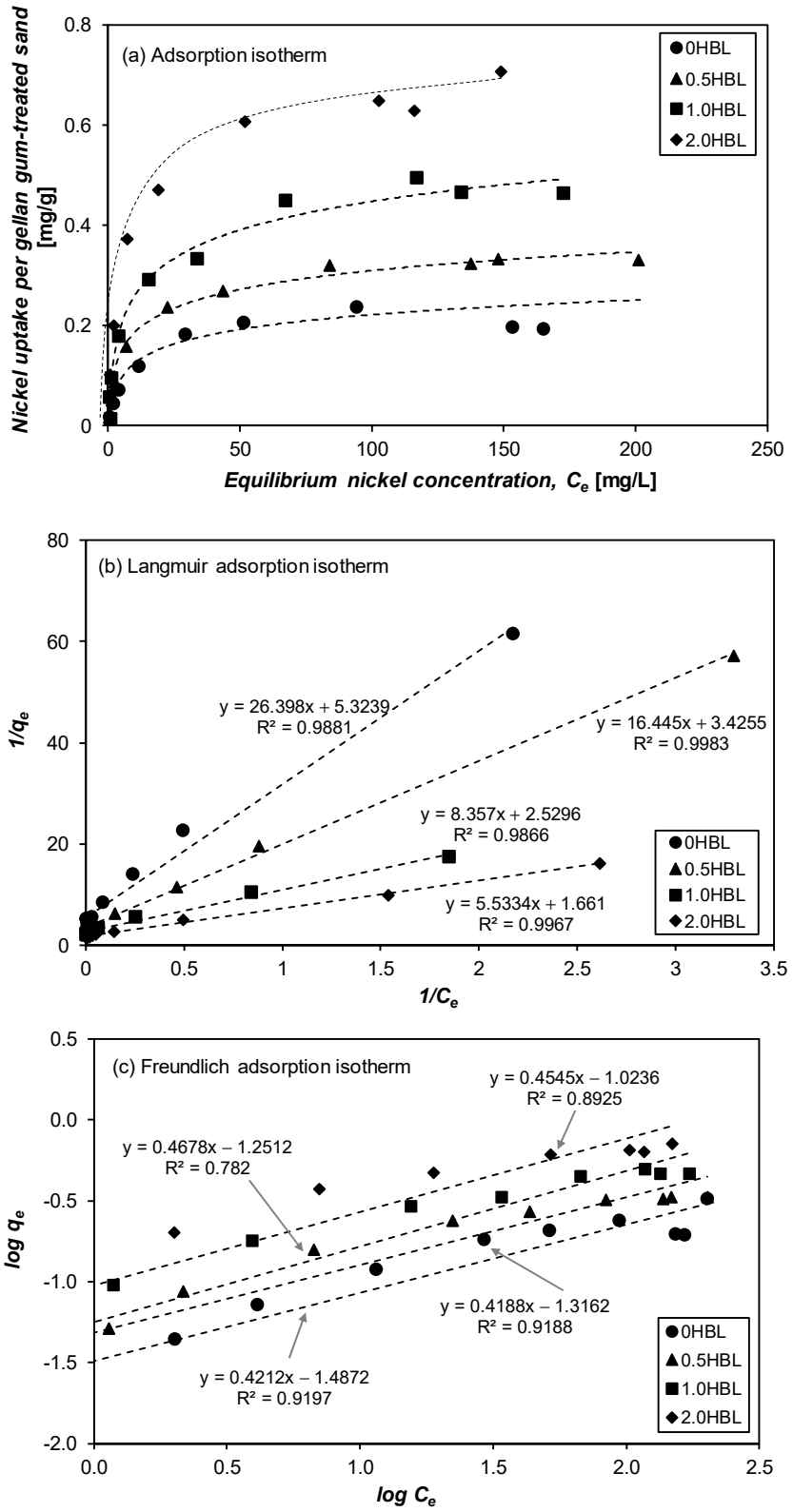

Figure 4. Adsorption isotherm at various initial nickel concentrations (10–1000 mg/L) on gellan gum-treated sand (**a**), the Langmuir adsorption isotherm (**b**), and the Freundlich adsorption isotherm of nickel on sample (**c**).

Table 3. Parameters of the Langmuir model and the Freundlich model.

Parameters	0 HBL	0.5 HBL	1.0 HBL	2.0 HBL
		Langmuir isotherm		
q_{max}	0.19	0.29	0.40	0.60
k_L	0.20	0.21	0.30	0.30
R^2	0.9881	0.9983	0.9866	0.9967
		Freundlich isotherm		
k_F	0.03	0.05	0.06	0.09
N	2.37	2.39	2.14	2.20
R^2	0.9197	0.9188	0.782	0.8925

The adsorption of Ni^{2+} on GG and sand indicated monolayer coverage of the adsorbate on the surface of the adsorbent, which is coherent with that of other studies on heavy metal adsorption by biopolymers [21–23]. The Langmuir model is the best fitting model for the data set. The slope of Figure 4b was converted into q_{max} for a better understanding of the adsorption model. The q_{max} started from 0.19 mg/g for 0 HBL (pure sand) to 0.29 mg/g for 0.5 HBL, 0.40 mg/g for 1.0 HBL, and 0.60 mg/g for 2.0 HBL (Table 3). The results demonstrated that GG had a higher adsorbability compared with that of pure sand. The q_{max} increased with an increase in GG, which indicated that GG in HBL can improve the nickel adsorption ability of the entire HBL and can be the main adsorbent of the HBL system.

Kinetic study on Ni^{2+} adsorption by GG = 1% HBL with time shows an instantaneous increase in q_e and then steady-state after a specific time (Figure 5) [21,24]. The adsorption can be illustrated by two stages. In the first stage, there is rapid removal (regardless of the nickel concentration) within the first 1 min, and equilibrium is reached in the later stage in approximately 40 min. The rapid removal during the initial stage might be attributed to ample sites for adsorption on the surface of GG.

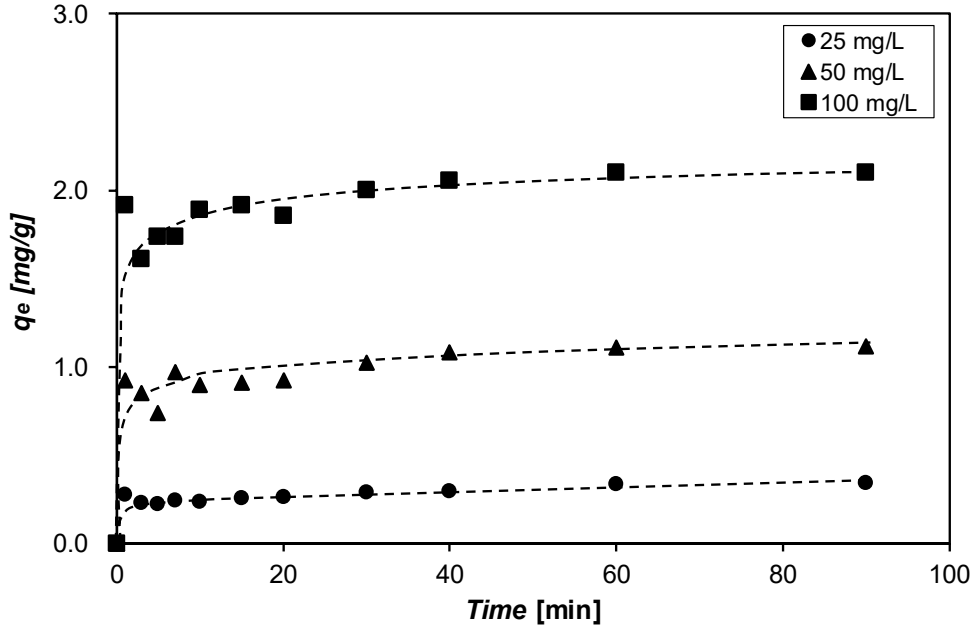

Figure 5. Kinetics of Ni^{2+} binding to the gellan gum (GG = 1.0% HBL) at different initial nickel ion concentrations of 25 mg/L, 50 mg/L, and 100 mg/L.

As shown in Figure 6, the SEM EDS spectra show peaks of GG in its pure state and nickel-adsorbed state. The EDS data show a reduction in the potassium peak and appearance of the nickel peak. This can be considered a cation exchange mechanism of GG

with Ni^{2+} ion, similar to that of other adsorbents [21]. The Ni^{2+} replacement for potassium in GG indicated that GG is a potassium-type GG [25,26]. Furthermore, the functional groups in GG (carbonyl, methylol, and methyl) were also responsible for chemical interaction with nickel ions [25]. Meanwhile, the sand can adsorb Ni^{2+} via the inner-sphere interaction, where Ni^{2+} can interact with silanol groups at the sand surfaces [27,28].

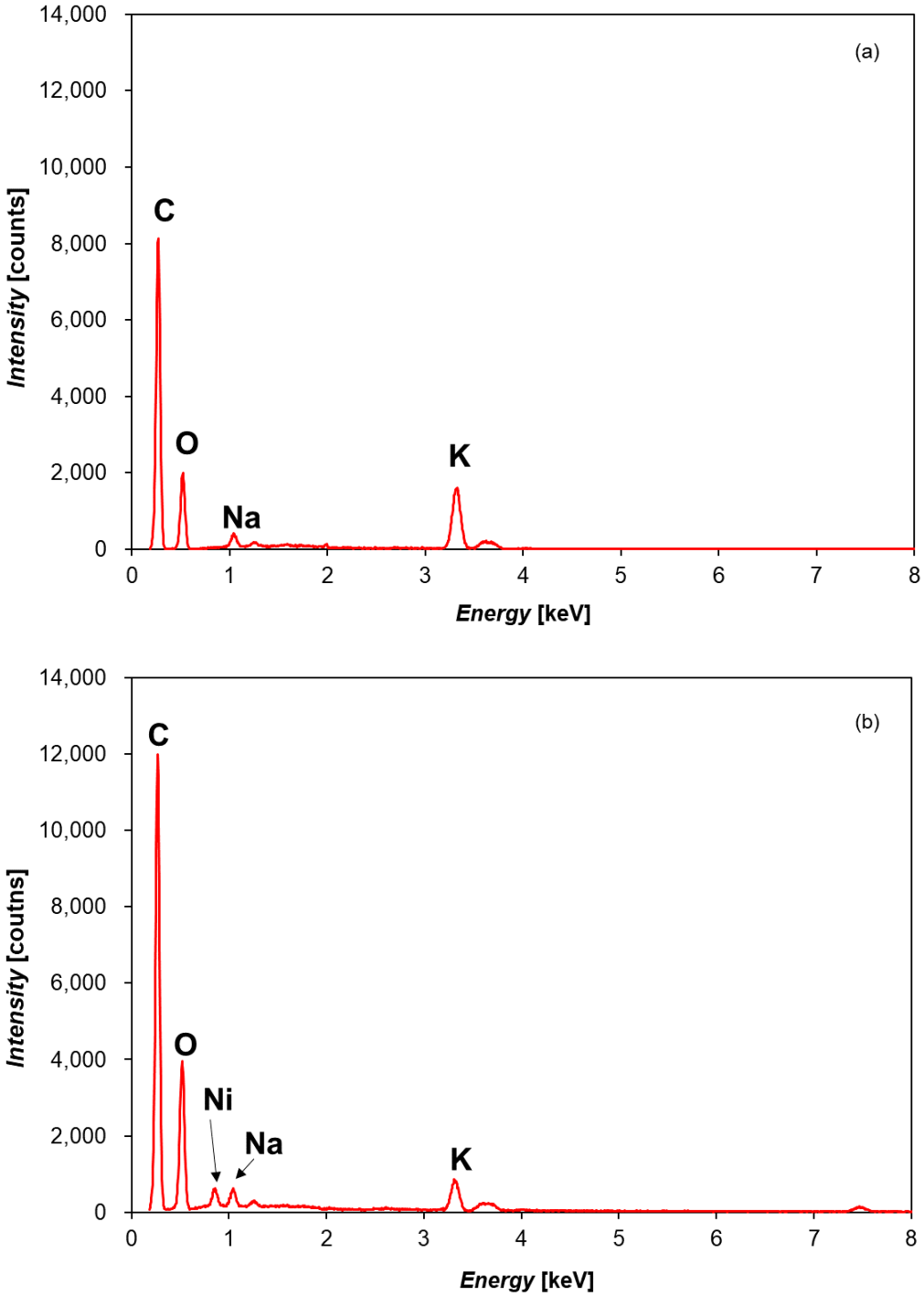

Figure 6. SEM-EDX spectra of (**a**) pure gellan gum and (**b**) nickel adsorbed gellan gum.

3.2. Isotherm and Kinetics of Ni^{2+} Adsorption Mechanism Control

The change in hydraulic conductivity with gellan gum content is shown in Figure 7. The hydraulic values of 0 HBL specimens were approximately 10^{-5} m/s regardless of

the magnitude of flow rate running through the specimens. Since HBLs were installed into the soil column, the initial hydraulic conductivity became lower than that of the hydraulic conductivity of the soil column without HBL. This was observed owing to the water absorption of GG. Furthermore, the hydraulic conductivity decreased with time due to the pore-clogging effect of GG [9] as GG interacted with water. The hydraulic conductivity decreased to 5.46×10^{-6}, 3.73×10^{-6}, and 6.02×10^{-7} m/s for 0.5, 1, and 2% GG, respectively, at a flow rate of 0.2 mL/min. Regarding the flow rate of 0.04 mL/min, the initial hydraulic conductivity (i.e., 1.32×10^{-5} m/s) decreased to 2.28×10^{-6}, 8.27×10^{-7}, and 4.19×10^{-7} m/s for 0.5, 1, and 2% GG, respectively.

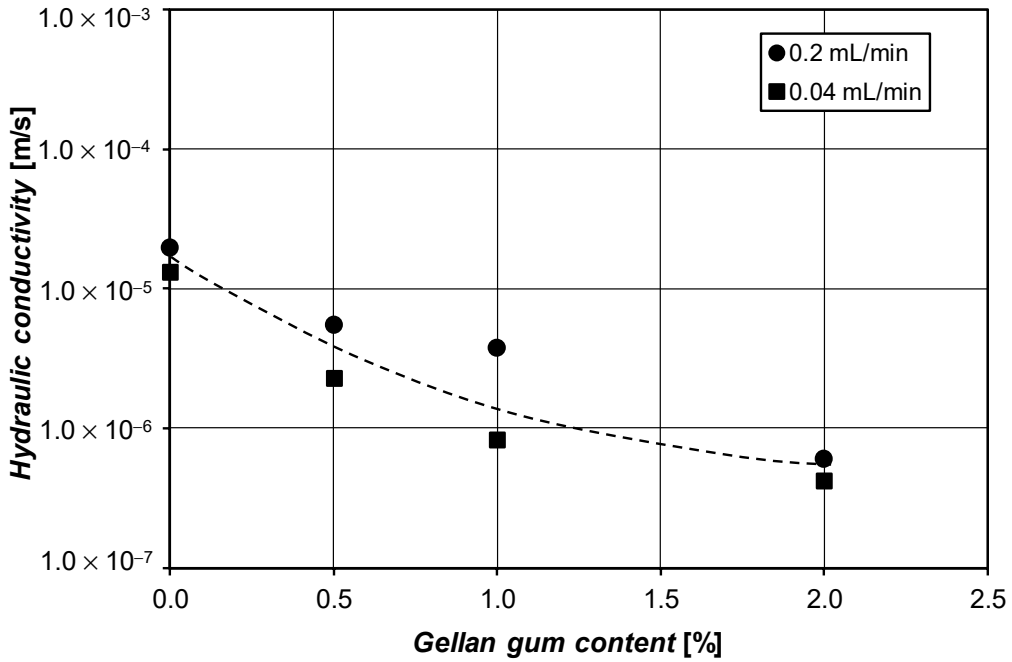

Figure 7. Change in the hydraulic conductivity of soil at flow rates of 0.04 mL/min and 0.2 mL/min.

The presence of meniscus water and free water in the sand column [29] caused the hydraulic behavior. The free water could be easily pushed out under the pressure-induced movement of the nickel-contaminated water, which formed water paths within the sand column. The formation of water paths also depended on the flow rate. The formation of water pathways was fast, with an increase in the flow rate. Therefore, the hydraulic conductivity values were 1.96×10^{-5} m/s and 1.31×10^{-5} m/s for flow rates of 0.2 mL/min and 0.04 mL/min, respectively.

As the HBL was installed, the water absorption of GG formed the hydrogel matrix in the pore space of HBL and caused the pore-clogging effect [9], which was essential to control the movement of the injected flow (nickel-contaminated water) in HBL. Furthermore, the flow rate affected the interaction between water molecules and GG hydrogel. A low injected flow rate (0.04 mL/min) could promote the pore-clogging effect earlier than a high injected flow rate (0.2 mL/min). With the occurrence of pore-clogging, the interaction between nickel and adsorbents increased.

3.3. Nickel Adsorption Behavior of Soil Column

In the cases of the 0 HBL, 0.5 HBL, and 1.0 HBL specimens, the Ni^{2+} adsorption behavior followed a similar trend to that when the Ni^{2+} solution was continuously supplied to the specimen. Initially, nickel ions were quickly adsorbed owing to the large amount of free exchangeable ions of absorbents. Subsequently, the adsorption reached equilibrium as the free sites for Ni^{2+} became less available due to the constant adsorption.

In general, the pure sand column had the lowest total amount of cumulative nickel adsorbed. GG in HBL improved the amount of Ni^{2+} removed from the Ni^{2+}-contaminated solution. A significant amount of nickel ion can be adsorbed with an increase in the GG content due to the increase in the functional groups and potassium cation exchange in the specimens provided by GG. The nickel adsorption trends (Figures 8 and 9) showed the potential maximal Ni^{2+} adsorption ability of specimens with different GG-treated sand at different flow rates. Total nickel adsorption varied proportionally with GG content.

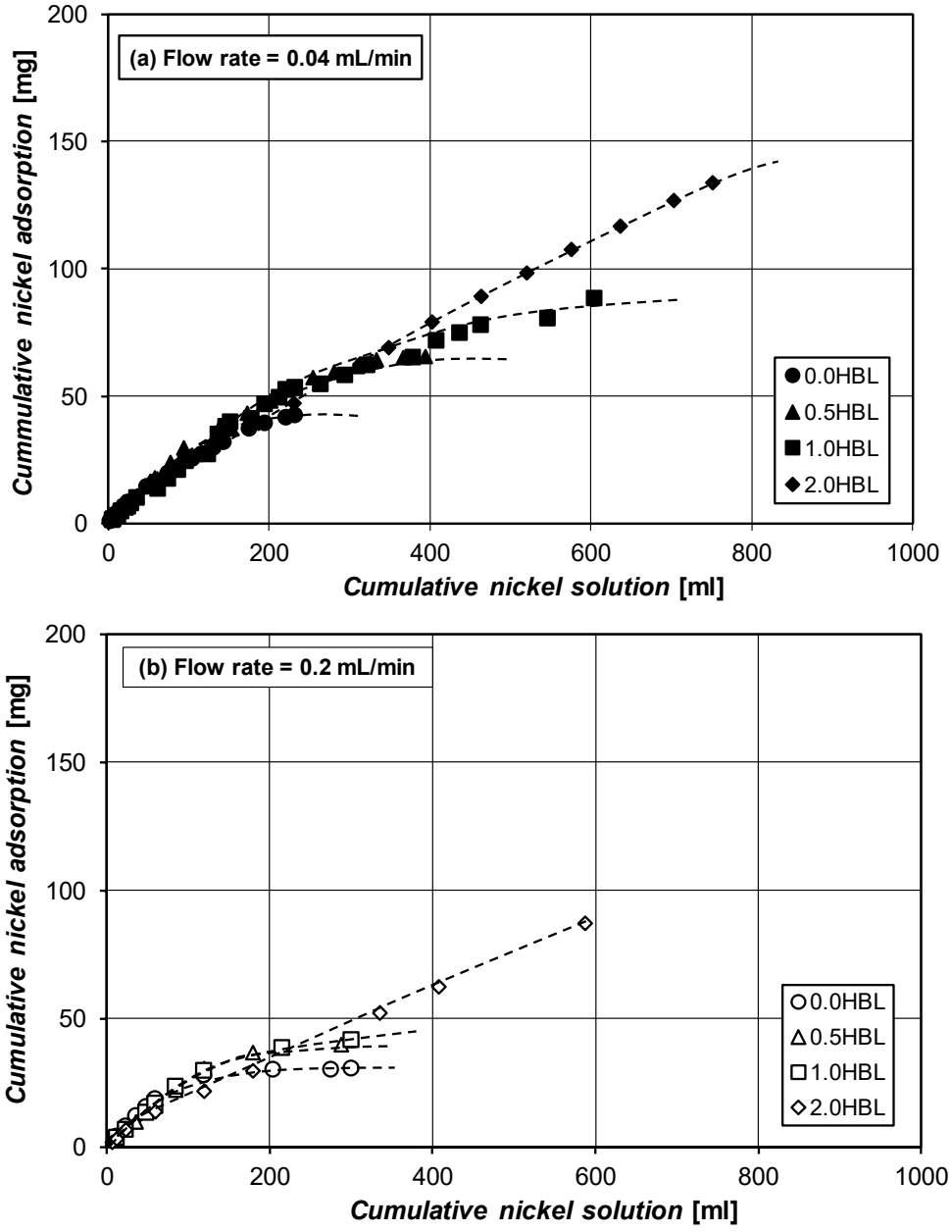

Figure 8. Effect of flow rate on removal efficiency of nickel adsorption.

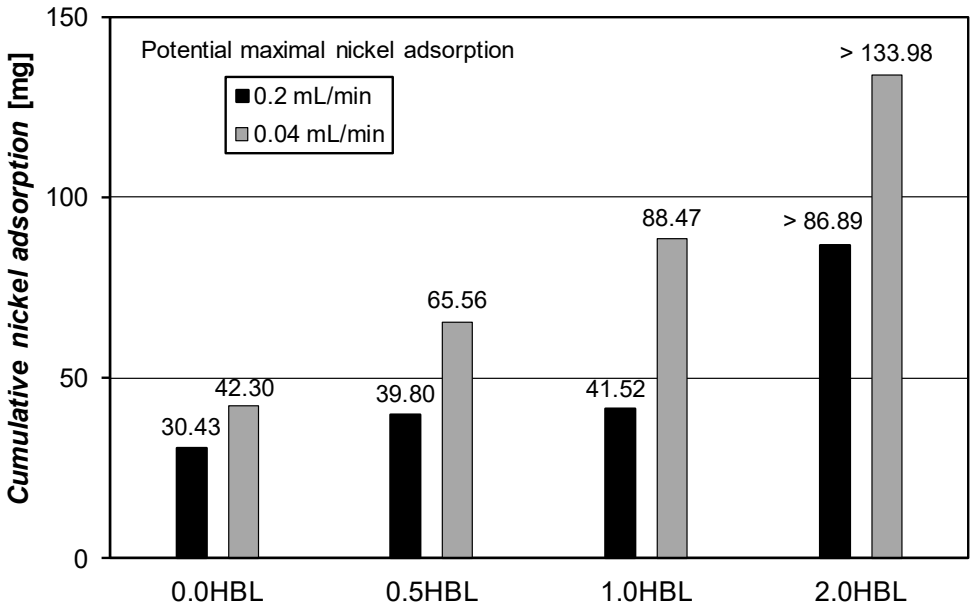

Figure 9. Potential maximal nickel adsorbability of specimens.

The flow rate was essential in controlling the contact time between Ni^{2+} and the adsorbent materials, which was crucial to determine the amount of nickel adsorbed. Therefore, there was a gap in the total amount of adsorbed Ni^{2+} obtained from the low and high flow rates. For instance, under a low flow rate (i.e., 0.04 mL/min), the 0 HBL specimen could adsorb 40 mg of Ni^{2+} ion as 200 mL of the Ni^{2+} solution flowed through the specimen (Figures 8a and 9). Conversely, 29.98 mg of Ni^{2+} was removed from the 200 mL nickel solution supplied at a high flow rate (0.2 mL/min) (Figures 8b and 9). This phenomenon also occurred in GG-treated sand. The 2.0 HBL adsorbed 86.89 mg and 133.98 mg nickel as 600 mL of the Ni^{2+} solution was provided at flow rates of 0.2 mL/min and 0.04 mL/min, respectively (Figures 8 and 9).

4. Discussion

This study shows an improvement in Ni^{2+} adsorption using GG-treated sand. The difference in the amount of adsorbed Ni^{2+} from the flows of 0.04 mL/min and 0.2 mL/min was determined by the GG content. To validate the practical applicability of GG-treated sand for heavy metal removal, the Ni^{2+} adsorption capacity of 1 m^3 GG-treated sand with different GG contents at the flow of 0.04 mL/min has been evaluated as shown in Figure 10.

The effect of hydraulic reduction with GG content decreases nonlinearly and levels off at a GG content of 1.0% [9]. However, if GG-treated sand is suggested for Ni^{2+} treatment, 2% gellan gum can significantly increase Ni^{2+} removal (Figure 9). To form 1 m^3 of the 2% GG–sand mixture, 26.5 kg GG should be dissolved in 463 L of heated water before mixing it with 1.3 tons of sand. If the GG–sand mixture is used to treat a 1 g/L Ni^{2+} contaminated flow of 0.04 mL/min, 1906 kg of nickel can be trapped by GG. The experiment was conducted within a given time. Therefore, 2% GG could not reach equilibrium. The amount of adsorbed Ni^{2+} by 1 m^3 GG-treated sand was calculated based on the experimental data. Therefore, the adsorbed Ni^{2+} becomes higher in a field application.

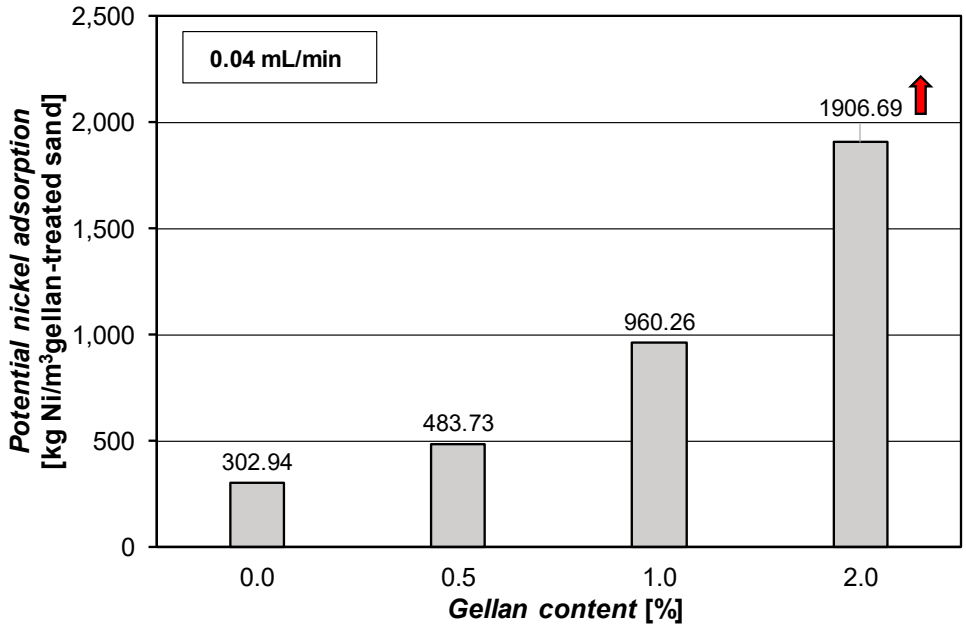

Figure 10. Potential nickel adsorption by 1 m^3 gellan gum-treated sand.

Recently, bentonite has been widely used owing to its high number of specific surfaces for hydraulic barriers, effective restriction of the migration of solutes, and significantly high adsorption of heavy metals [30,31]. However, bentonite causes side effects in humans (e.g., inhibiting hemolytic activity) and animals (e.g., damage to the lung epithelial cells of mice) [32–34]. A mixture including 10% bentonite and 90% sand is the most economical solution that satisfies the minimum requirement of hydraulic conductivity [35]. A mixture of bentonite-sand with a ratio of 1:9 (S9B1) was used as a 1 cm liner installed in the sand column. We observed that after 180 h subjected to the Ni^{2+}-contaminated solution at a flow rate of 0.04 mL/min, the removal efficiencies of 10BS, 2.0 HBL, 1.0 HBL, and 0.5 HBL were 60%, 53%, 36%, and 35%, respectively (Figure 11). The closest removal efficiency to that of 10BS was 2% GG. Therefore, high GG can be used as an alternative material for bentonite.

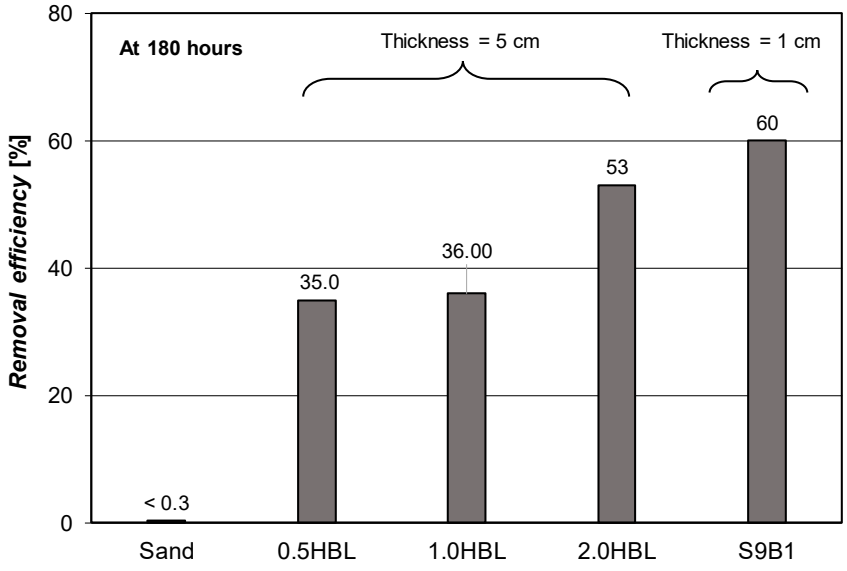

Figure 11. Comparison of the removal efficiency of pure sand, gellan gum-treated sand, and bentonite-treated sand.

The high cost of GG utilization for soil treatment compared with that of conventional hydraulic barrier materials such as bentonite is a severe concern for geotechnical engineers. For instance, 100 g of GG costs 217 USD [36], whereas 1 ton of bentonite costs approximately 75 USD [37]. However, owing to widespread usage in the food and cosmetic industries, the global GG market is expected to reach USD 62.96 million by 2023 from a market size of USD 50.257 million in 2017. Therefore, the use of GG for geotechnical application in general and for hydraulic barrier purposes is becoming increasingly feasible.

This study aimed to remove a concerning heavy metal with two valence electrons, nickel (Ni^{2+}), using GG-treated sand. One of the biggest advantages of the newly suggested GG–sand material is that it can be easily implemented in the field via direct mixing (e.g., GG–soil column mixing using an auger) or ground injection (e.g., GG solution grouting into porous ground). Implemented in situ, GG-treated sand layers (or barriers) are expected to enhance the ground strength in terms of shear strength and bearing capacity [14] in addition to reducing the ground water flow [9] and adsorbing hazardous Ni^{2+} from contaminated ground water. However, in order to bring GG-treated sand into practice, further study needs to be considered for other types of heavy metals and actual wastewater that contains different kinds of chemical pollutants.

5. Conclusions

To investigate the applicability of bio-soil treatment on Ni^{2+} removal, a series of Ni^{2+} adsorption tests were conducted on GG-treated jumunjin sand using a pressurized upward flow system. Additionally, adsorption isotherm and kinetic studies were performed to determine the possible mechanisms for Ni^{2+} adsorption. The main findings of this study are as follows:

- GG can improve the Ni^{2+} adsorption of sand by 150% or greater with the usage of 1% GG content or higher. The Langmuir model is the best fitting model for adsorption data of GG and sand. The potassium content within the GG mainly works on the cation exchange mechanism along with functional groups to interact with Ni^{2+}.
- GG enhances the Ni^{2+} removal efficiency of the sand column, controlled by GG content, and the flow rate via the interactions of water–GG, Ni^{2+}–GG, and Ni^{2+}–sand.
- The water absorption of GG causes the pore-clogging effect within the GG–sand system and, in turn, improves the Ni^{2+} removal efficiency. The pore-clogging effect was observed earlier in the process with an increase in the GG concentration.
- In general, GG shows a good performance for Ni^{2+} adsorption and pore-clogging effect, which controls the movement of flow rate and the amount of Ni^{2+} ion in the flow. Therefore, GG poses a promising alternative for hydraulic barriers.

Author Contributions: Conceptualization, T.P.A.T., H.C. and I.C.; experiment and analysis, T.P.A.T. and H.C.; writing—review and editing, T.P.A.T., H.C., G.-C.C., J.-I.H. and I.C. All authors have read and agreed to the published version of the manuscript.

Funding: This study was funded by the Ministry of Land, Infrastructure, and Transport (MOLIT) of the Korean Government, grant number 21AWMP-B114119-06.

Institutional Review Board Statement: Not applicable.

Informed Consent Statement: Not applicable.

Data Availability Statement: The data presented in this study are available upon request from the corresponding author.

Acknowledgments: This study was financially supported by the Water Management Research Program funded by the Ministry of Land, Infrastructure, and Transport (MOLIT) of the Korean Government (21AWMP-B114119-06) and the New Faculty Research Fund of Ajou University.

Conflicts of Interest: The authors declare no conflict of interest.

References

1. Kelly, J.; Thornton, I.; Simpson, P. Urban geochemistry: A study of the influence of anthropogenic activity on the heavy metal content of soils in traditionally industrial and non-industrial areas of Britain. *Appl. Geochem.* **1996**, *11*, 363–370. [CrossRef]
2. Radziemska, M.; Mazurb, Z.; Jeznacha, J. Influence of applying halloysite and zeolite to soil contaminated with nickel on the content of selected elements in Maize (*Zea mays* L.). *Chem. Eng.* **2013**, *32*, 301–306. [CrossRef]
3. Balkaya, M. Evaluation of the use of alum sludge as hydraulic barrier layer and daily cover material in landfills: A finite element analysis study. *Desalin. Water Treat.* **2016**, *57*, 2400–2412. [CrossRef]
4. Prashanth, J.P.; Sivapullaiah, P.V.; Sridharan, A. Pozzolanic fly ash as a hydraulic barrier in land fills. *Eng. Geol.* **2001**, *60*, 245–252. [CrossRef]
5. Bassi, R.; Prasher, S.O.; Simpson, B. Removal of selected metal ions from aqueous solutions using chitosan flakes. *Sep. Sci. Technol.* **2000**, *35*, 547–560. [CrossRef]
6. Lázaro, N.; Sevilla, A.L.; Morales, S.; Marqués, A.M. Heavy metal biosorption by gellan gum gel beads. *Water Res.* **2003**, *37*, 2118–2126. [CrossRef]
7. Mogollon, L.; Rodriguez, R.; Larrota, W.; Ramirez, N.; Torres, R. Biosorption of nickel using filamentous fungi. In *Biotechnology for Fuels and Chemicals*; Humana Press: Totowa, NJ, USA, 1998; pp. 593–601.
8. Zhang, L.; Zeng, Y.; Cheng, Z. Removal of heavy metal ions using chitosan and modified chitosan: A review. *J. Mol. Liq.* **2016**, *214*, 175–191. [CrossRef]
9. Chang, I.; Im, J.; Cho, G.-C. Geotechnical engineering behaviors of gellan gum biopolymer treated sand. *Can. Geotech. J.* **2016**, *53*, 1658–1670. [CrossRef]
10. Bouazza, A.; Gates, W.; Ranjith, P. Hydraulic conductivity of biopolymer-treated silty sand. *Géotechnique* **2009**, *59*, 71–72. [CrossRef]
11. Fourest, E.; Volesky, B. Alginate properties and heavy metal biosorption by marine algae. *Appl. Biochem. Biotechnol.* **1997**, *67*, 215–226. [CrossRef]
12. Mani, S.; Khabaz, F.; Godbole, R.V.; Hedden, R.C.; Khare, R. Structure and hydrogen bonding of water in polyacrylate gels: Effects of polymer hydrophilicity and water concentration. *J. Phys. Chem. B* **2015**, *119*, 15381–15393. [CrossRef] [PubMed]
13. Aal, G.Z.A.; Atekwana, E.A.; Atekwana, E.A. Effect of bioclogging in porous media on complex conductivity signatures. *J. Geophys. Res. Biogeosci.* **2010**, *115*, 1–10. [CrossRef]
14. Chang, I.; Cho, G.-C. Shear strength behavior and parameters of microbial gellan gum-treated soils: From sand to clay. *Acta Geotech.* **2019**, *14*, 361–375. [CrossRef]
15. Staerkjaer, L.; Menné, T. Nickel allergy and orthodontic treatment. *Eur. J. Orthod.* **1990**, *12*, 284–289. [CrossRef]
16. Wong, S.; Fournier, M.; Coderre, D.; Banska, W.; Krzystyniak, K. Environmental immunotoxicology. In *Animal Biomarkers as Pollution Indicators*; Springer: Dordrecht, The Netherlands, 1992; pp. 167–189.
17. World Health Organization; International Agency for Research on Cancer. *Tobacco Smoke and Involuntary Smoking*; World Health Organization: Geneva, Switzerland, 2004.
18. Osmałek, T.; Froelich, A.; Tasarek, S. Application of gellan gum in pharmacy and medicine. *Int. J. Pharm.* **2014**, *466*, 328–340. [CrossRef] [PubMed]
19. Rathor, G.; Chopra, N.; Adhikari, T. Nickel as a pollutant and its management. *Int. Res. J. Environ. Sci.* **2014**, *3*, 94–98.
20. Krishnan, K.A.; Sreejalekshmi, K.; Baiju, R. Nickel (II) adsorption onto biomass based activated carbon obtained from sugarcane bagasse pith. *Bioresour. Technol.* **2011**, *102*, 10239–10247. [CrossRef]
21. Panda, G.; Das, S.; Bandopadhyay, T.; Guha, A. Adsorption of nickel on husk of Lathyrus sativus: Behavior and binding mechanism. *Colloids Surf. B Biointerfaces* **2007**, *57*, 135–142. [CrossRef]
22. Huang, C.; Chung, Y.-C.; Liou, M.-R. Adsorption of Cu (II) and Ni (II) by pelletized biopolymer. *J. Hazard. Mater.* **1996**, *45*, 265–277. [CrossRef]
23. Stojakovic, D.; Milenkovic, J.; Daneu, N.; Rajic, N. A study of the removal of copper ions from aqueous solution using clinoptilolite from Serbia. *Clays Clay Miner.* **2011**, *59*, 277–285. [CrossRef]
24. Panda, G.; Das, S.; Chatterjee, S.; Maity, P.; Bandopadhyay, T.; Guha, A. Adsorption of cadmium on husk of Lathyrus sativus: Physico-chemical study. *Colloids Surf. B Biointerfaces* **2006**, *50*, 49–54. [CrossRef]
25. Kawahara, S.; Yoshikawa, A.; Hiraoki, T.; Tsutsumi, A. Interactions of paramagnetic metal ions with gellan gum studied by ESR and NMR methods. *Carbohydr. Polym.* **1996**, *30*, 129–133. [CrossRef]
26. Tsutsumi, A.; Ya, D.; Hiraoki, T.; Mochiku, H.; Yamaguchi, R.; Takahashi, N. ESR studies of Mn (II) binding to gellan and carrageenan gels. *Food Hydrocoll.* **1993**, *7*, 427–434. [CrossRef]
27. Awan, M.A.; Qazi, I.A.; Khalid, I. Removal of heavy metals through adsorption using sand. *J. Environ. Sci.* **2003**, *15*, 413–416.
28. Takahashi, N.; Kuroda, K. Materials design of layered silicates through covalent modification of interlayer surfaces. *J. Mater. Chem.* **2011**, *21*, 14336–14353. [CrossRef]
29. Karube, D.; Kawai, K. The role of pore water in the mechanical behavior of unsaturated soils. *Geotech. Geol. Eng.* **2001**, *19*, 211–241. [CrossRef]
30. Di Emidio, G.; Mazzieri, F.; Verastegui-Flores, R.D.; Van Impe, W.; Bezuijen, A. Polymer-treated bentonite clay for chemical-resistant geosynthetic clay liners. *Geosynth. Int.* **2015**, *22*, 125–137. [CrossRef]

31. Mohajeri, P.; Smith, C.; Selamat, M.; Abdul Aziz, H. Enhancing the Adsorption of Lead (II) by Bentonite Enriched with pH-Adjusted Meranti Sawdust. *Water* **2018**, *10*, 1875. [CrossRef]
32. Adamis, Z.; Fodor, J.; Williams, R. *Environmental Health Criteria 231: Bentonite, Kaolin and Selected Clay Minerals*; World Health Organization, International Programme on Chemical Safety: Geneva, Switzerland, 2005.
33. Geh, S.; Shi, T.; Shokouhi, B.; Schins, R.P.; Armbruster, L.; Rettenmeier, A.W.; Dopp, E. Genotoxic potential of respirable bentonite particles with different quartz contents and chemical modifications in human lung fibroblasts. *Inhal. Toxicol.* **2006**, *18*, 405–412. [CrossRef] [PubMed]
34. Gibbs, A.; Pooley, F. Fuller's earth (montmorillonite) pneumoconiosis. *Occup. Environ. Med.* **1994**, *51*, 644–646. [CrossRef]
35. Alkaya, D.; Esener, A.B. Usability of sand-bentonite-cement mixture in the construction of unpermeable layer. *Sci. Res. Essays* **2011**, *6*, 4492–4503. [CrossRef]
36. Sigma-Aldrich. Gelzan™ CM. Available online: https://www.sigmaaldrich.com/catalog/search?term=gellan+gum&interface=All&N=0&mode=partialmax&lang=ko&region=KR&focus=product (accessed on 29 April 2019).
37. Statista. Average Bentonite Price in the U.S. from 2007 to 2018. Available online: https://www.statista.com/statistics/248186/average-bentonite-price/ (accessed on 29 April 2019).